Theor Chem Acc (2012) 131:1225
DOI 10.1007/s00214-012-1225-8

REGULAR ARTICLE

Theoretical and experimental investigation on the near-infrared and UV–vis spectral regions of a newly synthesized triarylamine electrochromic system

Bruna Clara De Simone · Angelo Domenico Quartarolo · Sante Cospito · Lucia Veltri · Giuseppe Chidichimo · Nino Russo

Received: 17 January 2012 / Accepted: 18 April 2012 / Published online: 8 May 2012

Abstract A new triarylamine derivative, *N,N′*-Bis (4-heptanoylamidophenyl)-*N,N′*-di(4-methoxyphenyl)-1,4-phenylenediamine, with stable electrochromism in near-infrared and visible light regions, has been synthesized and characterized at theoretical and experimental level. The detected and simulated spectra, with and without the presence of an external potential at different values, clearly show that this mixed-valence system undergoes ionization at a low value of the applied potential, and the formed radical cation absorbs in the near-infrared region with an intense peak located at 1,040 nm. Density functional computations give the geometrical structure and absorption properties in very good agreement with experiment, allowing assigning the electronic transition and contributing to an understanding of the electron-transfer process between the two redox centers.

Keywords Electrochromism · Density functional theory · Electron transfer · Mixed-valence compound

Dedicated to Professor Vincenzo Barone and published as part of the special collection of articles celebrating his 60th birthday.

Electronic supplementary material The online version of this article (doi:10.1007/s00214-012-1225-8) contains supplementary material, which is available to authorized users.

B. C. De Simone (✉) · A. D. Quartarolo · S. Cospito · L. Veltri · G. Chidichimo · N. Russo (✉)
Dipartimento di Chimica, Università della Calabria, 87036 Rende, CS, Italy
e-mail: desimone@unical.it

N. Russo
e-mail: nrusso@unical.it

1 Introduction

Electrochromism is the property of a material to reversibly change color in response to an externally applied potential: this effect is connected with the use of electrochromic (EC) molecules, whose UV–visible spectrum exhibits new optical absorption bands when an electron is gained or lost in a redox process [1, 2]. Recently the "electrochromic" definition has been extended to molecules that show modulation of radiation in the near-infrared (NIR) or microwave regions, and "color" can mean response of detectors to these wavelengths, not just of the human eye. In the last years, different molecular systems that show interesting electrochromic behavior have been synthesized, characterized, and proposed for a series of applications [3–6]. Special interest [7] has been devoted to the mixed-valence (MV) systems containing more than one redox state in the same molecule or molecular unit. These systems play an important role in the study of the intramolecular electron transfer called intervalence transfer (IT) by Hush [8]. In MV molecules, IT bands are typically formed in the NIR region from 1,000 to 2,000 nm.

Generally, the used organic or inorganic MV compounds contain at least two redox states linked throughout by bridged molecules and assume a mono-dimensional topology. The properties of MV species essentially depend on the extend of electronic interaction between the redox centers and have been classified by Robin and Day [9] on the basis of this characteristic as negligible (Class I), moderate (Class II), and strong (Class III). Among the proposed organic MV systems that contain *N,N,N′,N′*-tetraphenyl-*p*-phenylenediamine units are particularly interesting for NIR applications because of their intramolecular electron transfer in the oxidized states [10]. The major part of the studies available in the literature on these systems

concerns the *N,N,N′,N′*-tetraphenyl-*p*-phenylenediamine (TPPA), for which X-ray diffraction, electrochemical, spectroscopic, and theoretical data are available [11–15]. Furthermore, experimental and theoretical studies on a series of substituted triarylamine redox systems including fluorine-based conjugated polymers containing propeller-shape di-triarylamine with electron-donating propylphenyl groups and other chemical substituents have been recently published [10, 16–22]. Despite these studies, we are far from an exhaustive knowledge of the elementary mechanism that explains the electron-transfer reactions that occur in the mixed-valence systems. More experimental and theoretical works are required to fully explain the phenomenon as well as to propose efficient new molecules with electrochromic properties. In this context and with the aim to contribute to the clarification of the electron-transfer process and to design new systems active in the near-infrared band region, a novel highly stable molecule based on the electroactive tetraphenyl-*p*-phenylenediamine unit, *N,N′*-Bis(4-heptanoylamidophenyl)-*N,N′*-di(4-methoxyphenyl)-1,4-phenylenediamine (TPPAHM) (Scheme 1), has been synthesized and investigated through UV–vis–NIR spectroscopy and density functional theory (DFT) calculations. Our strategy is to incorporate electron-donating substituents at the *para* position of the phenyl groups in order to greatly prevent the coupling reactions by affording stable cation radical [10]. Moreover, the methoxy and amide groups para-substituted make this molecule readily soluble in polar aprotic solvents. The main characteristic of this new triarylamine is the presence of a strong peak in the NIR region when an external electric field is applied. In addition to the applications as smart windows, car mirrors, and display panels [23–25], this NIR EC molecule could be exploitable for heating control in buildings. In this paper, we present the experimental (UV–vis—NIR spectra upon increasing electric field) and theoretical characterization (time-dependent–density functional theory, TD-DFT, spectral simulation) of TPPAHM. In addition, for the purpose of comparison, we report also new spectra and their theoretical analysis for the TPPA system.

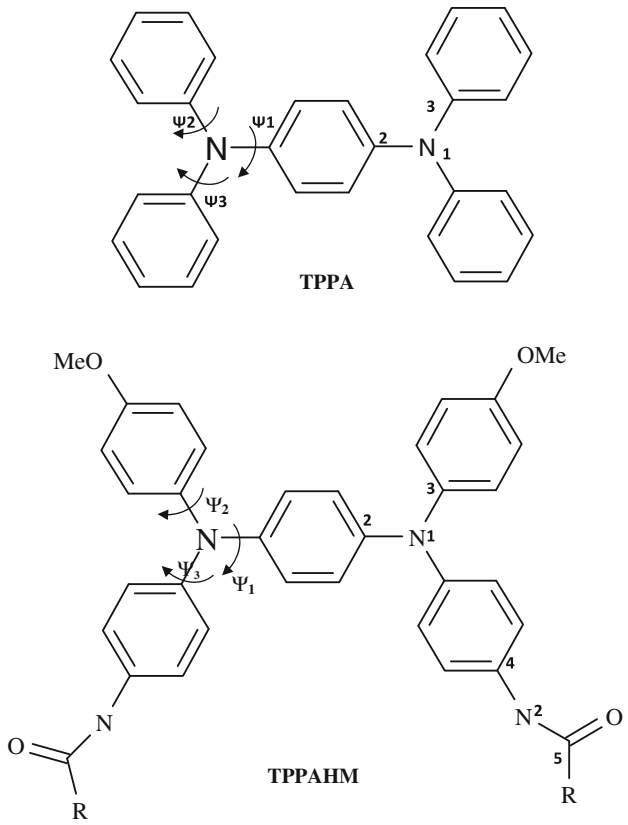

Scheme 1 Molecular structures for TPPA and TPPAHM with main bond length and torsional angle (Ψ_1–Ψ_3) labeling. R = –CH_3 and R = –$(CH_2)_5CH_3$ are the substituent groups, respectively, for the model and real systems

2 Experimental and theoretical details

2.1 Synthesis

N,N′-Bis(4-nitrophenyl)-*N,N′*-di(4-methoxyphenyl)-1,4-phenylenediamine was prepared by Ullmann coupling between 1,4-di-iodobenzene and 4-methoxy-4′-nitrodiphenylamine according to previously published procedures [10]. *N,N′*-Bis(4-heptanoylamidophenyl)-*N,N′*-di(4-methoxyphenyl)-1,4-phenylenediamine was prepared in a two-step procedure as described below. All other materials were commercially available and were used without further purification. In a 250-mL three-neck round-bottomed flask equipped with a stirring bar under nitrogen atmosphere, *N,N′*-Bis(4-nitrophenyl)-*N,N′*-di(4-methoxyphenyl)-1,4-phenylenediamine (1.01 g, 1.79 mmol) was dissolved in 10 mL of ethanol and 60 mL of tetrahydrofurane (THF). To the stirred solution was slowly added hydrazine monohydrate (1 g, 20.0 mmol), and the mixture was refluxed. Just when it began to reflux, Raney Ni (about 100 mg) was added. The solution frothed, and as the reaction proceeded, the color changed from yellow to almost colorless. After further 6 h of heating, the hot solution was filtered under nitrogen to remove Raney Ni, and the filtrate was washed with THF. The THF was removed by distillation at 65–70 °C under nitrogen atmosphere. The remaining ethanol solution was cooled to 0 °C under nitrogen in order to have the precipitation of crude *N,N′*-Bis(4-aminophenyl)-*N,N′*-di(4-methoxyphenyl)-1,4-phenylenediamine that was recovered by filtration, washed with cold ethanol, and dried in vacuum. The *N,N′*-Bis(4-aminophenyl)-*N,N′*-di(4-methoxyphenyl)-1,4-phenylenediamine was unstable and was immediately used in the next step without further purification. To a stirred solution

of crude *N,N′*-Bis(4-aminophenyl)-*N,N′*-di(4-methoxyphenyl)-1,4-phenylenediamine, prepared as described above, in 16 mL of dry THF, 0.9 mL of NEt_3 was added under nitrogen. To the resulting mixture, a solution of heptanoyl chloride (0.46 mL, 2.98 mmol) in 11 mL of dry THF was dropped, and the mixture was stirred at room temperature. After 20 h, a colorless precipitate was formed. The precipitate was collected by filtration, washed with cold ethanol, and dried in vacuum to give 0.58 g (45 % based on starting *N,N′*-Bis(4-nitrophenyl)-*N,N′*-di(4-methoxyphenyl)-1,4-phenylenediamine) of crude *N,N′*-Bis(4-heptanoylamidophenyl)-*N,N′*-di(4-methoxyphenyl)-1,4-phenylenediamine, TPPAHM, that was sufficiently pure by TLC (silica gel 60 F_{254}; 1:1 Hexane-AcOEt) and NMR analysis and was used without further purification. Mp 218–221 °C; IR (KBr): ν = 3,303 (m), 2,976 (m), 2,938 (m), 2,756 (m), 2,758 (m), 2,677 (m), 2,491 (m), 1,657 (s), 1,505 (s), 1,398 (m), 1,171 (m), 1,036 (m), 805 (m) cm^{-1}; ^1H NMR (300 MHz, DMSO-d_6): δ = 0.86 (d, J = 6.4, 6 H), 1.24–1.40 (m, 8 H), 1.48–1.62 (m, 4 H), 2.21–2.34 (m, 8 H), 3.73 (s, 6 H), 6.80 (s, 4 H), 6.88 (d, J = 9.1, 4 H), 6.89 (d, J = 9.1, 4 H), 6.98 (d, J = 9.1, 4 H), 7.46 (d, J = 9.1, 4 H), 9.77 (s br, 2 H); MS (ESI^+, direct infusion): m/z = 749 $[(M + Na)^+]$; Anal. Calcd for $C_{46}H_{54}N_4O_4$ (726.95): C 76.00, H 7.49, N 7.71; found C 76.19, H, 7.47, N 7.73.

Melting point analyses were performed on a Linkam (LTS350 stage, TP94 System Controller) at a scan rate of 10 °C/min. ^1H NMR spectra were recorded at 25 °C on a Bruker DPX Avance 300 Spectrometer in DMSO-d_6 solutions at 300 MHz with Me_4Si as internal standard. IR spectra were taken with a JASCO FT-IR 4200 spectrometer, and microanalyses were carried out with a Carlo Erba Elemental Analyzed Mod. 1106. The electrospray ionization mass spectra were acquired by direct infusion on an ABSciex API 2000 mass spectrometer equipped with a turbo ion spray ionization source. The spectra in the positive ion mode were obtained under the following conditions: ion spray voltage (IS) 4,500 V; curtain gas 10 psi; temperature 25 °C; ion source gas (1) 20 psi; declustering and focusing potentials 50 and 400 V, respectively.

2.2 Electrochromic response

The electrochromic behavior of the two EC molecules was investigated by UV–vis–NIR spectroscopy.

Two solutions were prepared dissolving each molecule in aprotic organic solvents. The first solution was prepared dissolving TPPA in *N*-methyl-2-pyrrolidinone (NMP), while the second one is composed of TPPAHM dissolved in *N,N*-dimethylformamide (DMF). A small quantity of these solutions were introduced by capillarity in home-made cells, whose thickness was set to be about 30 μm by means of glass spheres. Cell walls had an indium tin oxide (ITO) conductive substrate in order to perform electro-optical characterization.

UV–vis–NIR spectra were recorded with a Thermo Scientific GENESYS 10S UV–Vis spectrophotometer. In our experimental setup, the cells have been powered by two electrodes fixed to the opposite extremes of the cell. The potential difference was supplied by means of an Amel 2049 model potentiostat. Measurements were performed at 25 °C.

In order to verify the oxidation reversibility, we applied to the sample a series of square potential pulses monitoring the absorbance at fixed wavelength (λ = 846 nm for TPPA and λ = 1,040 nm for TPPAHM) as a function of time. The absorbance increased during the pulse application and rapidly returned to its initial state once the pulse was removed.

2.3 Computational details

All calculations were performed with the TURBOMOLE V-6.0 software package [26]. Due to the medium–high molecular size of TPPAHM that requires high computational costs, the computation has been performed in a model system in which the $-(CH_2)_5CH_3$ moiety is substituted with the $-CH_3$ one. This substitution does not affect the spectral properties that are essentially due to the aromatic core. Geometry optimizations, without imposing symmetry constraints, as well as vibrational frequency analysis were carried out at the density functional level of theory in conjunction with the non-empirical PBE0 hybrid functional [27, 28] that adds up a fixed amount of Hartree–Fock exchange energy (25 %) to the gradient-corrected PBE exchange–correlation functional. The SV(P) double-ζ quality basis set containing polarization functions on C, N, and O atoms ([3s2p1d]/[2s]) of Ahlrichs et al. [29, 30] was used for all the computations. Vibrational frequency analysis confirmed each optimized structure as absolute energy minimum on the relative potential energy surfaces. The closed-shell systems (neutral species) were treated with the restricted Kohn–Sham (RKS) formalism, while for the open-shell systems (cation and di-cation species), unrestricted Kohn–Sham (UKS) calculations were performed. For the open-shell compounds, the $\langle S^2 \rangle$ values of the ground-state Kohn–Sham determinant computed at the PBE0/SV(P) level of theory were found in the range 0.76–0.77 (for the cation) and 2.02–2.05 (for the di-cation), indicating a small effect of spin contamination. The lowest twenty vertical excitation energies were calculated by time-dependent density-functional linear response theory [31, 32] (TD-DFT) on the PBE0/SV(P) optimized geometries. The reliability of the excitation energies obtained from the combination of SV(P) basis set and hybrid functional (PBE0) has been previously tested for a series of molecular

Table 1 Main geometrical parameters for TPPA and TPPAHM neutral, radical cation, and di-cation species

Parameter	TPPA	$TPPA^+$	$TPPA^{2+}$	TPPAHM	$TPPAHM^+$	$TPPAHM^{2+}$
N1–C2	1.412 (1.433)	1.374 (1.363)	1.419	1.410	1.380	1.418
N1–C3	1.410 (1.404)	1.422 (1.444)	1.399	1.408	1.415	1.400
C4–N2	/	/	/	1.403	1.390	1.371
N2–C5	/	/	/	1.506	1.510	1.409
C5–O	/	/	/	1.371	1.385	1.204
C2–N1–C3	119.8 (116.9)	121.1 (120.9)	119.7	119.5	120.7	119.5
Ψ_1	41.8 (53.8)	24.7 (16.0)	43.0	40.7	26.9	43.6
Ψ_2	40.1 (55.7)	48.5 (49.1)	36.4	44.5	48.6	38.2
Ψ_3	39.4 (23.0)	48.4 (64.8)	36.5	37.6	44.5	34.2

Distances are in Å, and valence and dihedral angles in degree. The experimental results (from ref. [11]) are given in parenthesis

systems, giving a mean absolute deviation from experiment within 0.2–0.3 eV [33–37]. Solvent effects on geometries and excitation energies, due to electrostatic interaction in polar solvent, were taken into account with the conductor-like screening model [38, 39] assuming the dielectric constant value of 37.2 and 32.2 for DMF and NMP, respectively, and default parameters for the cavity generation. The simulation of the electronic spectra band profile was obtained by a sum of Gaussian shape functions centred at each excitation energy and with a constant full width at half maximum of 0.3 eV.

Default threshold for the geometry optimizations and for XC grid integrations has been used. In short, the used protocol is very similar to that suggested by Renz et al. [40] for the study of mixed-valence radical cations.

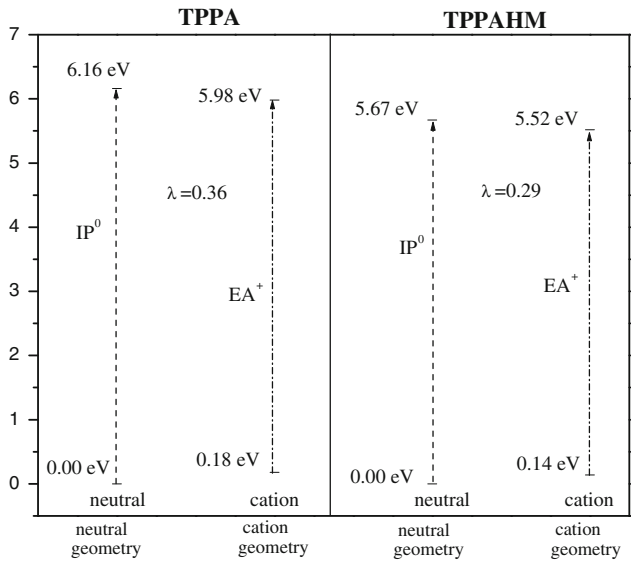

Fig. 1 Vertical and adiabatic relative energies (eV) at neutral and cation geometries for TPPA and TPPAHM molecules. For each compound, the neutral geometry is taken as energy reference. IP^0, EA^+, and λ are the ionization potentials (at neutral geometry), electron affinity (at cation geometry), and the reorganization energy

3 Results and discussion

The two studied molecules are shown in Scheme 1. Both show N–N distance of 5.654 Å, and a number of bonds linking the redox center equal to 5. Following the indication of Nelsen et al. [41], even though the distance between the two redox centers is short, these species can have a

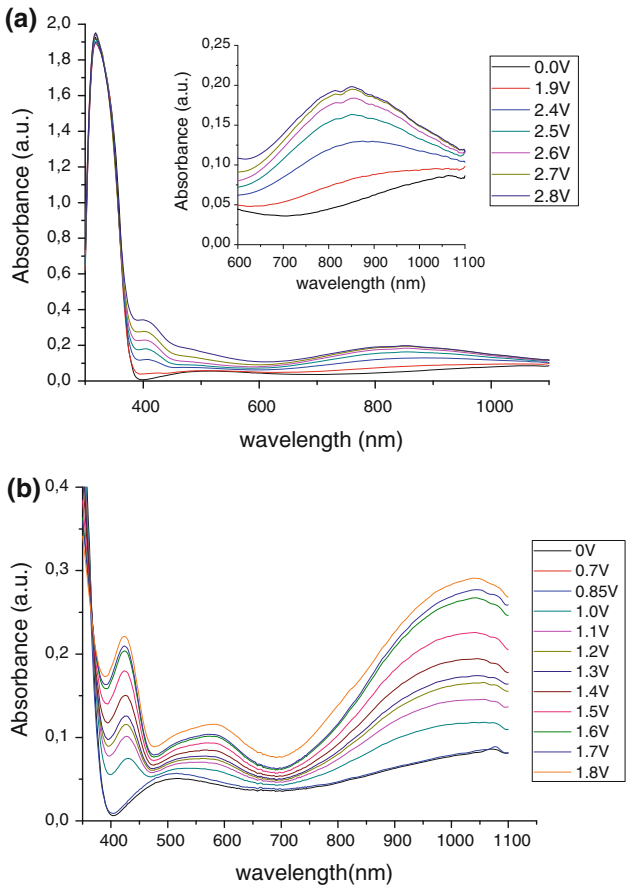

Fig. 2 **a** vis–NIR absorption spectra of 30 mM TPPA in NMP solution under different applied potentials; **b** vis–NIR absorption spectra of 1.5 mM TPPAHM in DMF solution under different applied potentials

Table 2 Computed vertical excitation energies, main configuration, and oscillator strengths *f* for molecule TPPA in *N*,*N*-dimethylformamide ($\varepsilon = 37.2$) and molecule TPPAHM in *N*-methyl-2-pyrrolidinone ($\varepsilon = 32.2$)

TPPA				TPPAHM			*Exptl.*
State	ΔE (eV, nm)	Main configuration (%)	*f*	ΔE (eV, nm)	Main configuration (%)	*f*	
1	3.65, 338	H → L (94.7)	0.0102	3.40, 365	H → L (95.6)	0.0046	318 (1.9257)
2	3.70, 335	H → L + 1 (97.6)	0.6169	3.48, 356	H → L + 1 (93.7)	0.7344	
3	3.97, 312	H → L + 2 (93.7)	0.1988	3.71, 335	H → L + 2 (84.0)	0.0192	
4	3.99,311	H → L + 3 (56.5)	0.0385	3.78, 328	H → L + 2 (94.0)	0.3432	
5	4.04, 307	H → L + 4 (50.9)	0.1608	3.88, 319	H → L + 3 (90.4)	0.3094	
Cation							
1	1.47, 842	H-1 → L β (96.8)	0.4247	1.21, 1025	H-1 → L β (97.9)	0.4812	848 (0.1983)
2	2.42, 513	H-6 → L β (69.6)	0.0038	2.09, 593	H-3 → L β (97.5)	0.0520	
3	2.46, 504	H-3 → L β (97.6)	0.0000	2.14, 580	H-4 → L β (97.8)	0.1668	
4	2.66, 466	H-9 → L β (97.7)	0.0176	2.63,471	H-17 → L β (63.2)	0.0004	
5	3.37, 368	H → L + 1 α (74.3)	0.3800	3.14, 395	H → L + 1 α (43.7)	0.2058	
Di-cation							
1	1.69, 733	H-3 → L β (83.6)	0.0272	1.53, 810	H-2 → L β (95.0)	0.1916	
2	1.72, 721	H-4 → L + 1 β (81.8)	0.0000	1.58, 786	H-3 → L β (93.9)	0.2547	
3	1.77, 699	H-2 → L β (66.7)	0.0262	2.03, 611	H-2 → L + 1 β (92.9)	0.0927	
4	1.88, 658	H-10 → L β (59.3)	0.1911	2.07, 599	H-3 → L + 1 β (94.3)	0.0823	
5	2.02, 615	H-8 → L β (58.8)	0.1022	2.11, 588	H-6 → L β (87.1)	0.2745	
6	2.05, 605	H-5 → L β (64.8)	0.1276	2.23, 556	H-11 → L β (71.3)	0.0003	
7	2.29, 541	H-14 → L β (86.1)	0.2404	2.24, 553	H-12 → L β (67.3)	0.0333	

good electronic coupling due to the presence of the five interlink bonds.

The computed and measured properties will be reported and discussed in specific sections.

3.1 Structural properties

The main geometrical parameters for the ground state of the neutral, cationic, and bi-cationic species of both the considered systems are reported in Table 1. The molecular structures computed with and without symmetry constraints are almost identical. In all cases, the nitrogen centers, surrounded by the three phenyl groups, are trigonal planar, and the CNC valence angle values are about 120°. This means that the central nitrogen atoms are sp^2 hybridized, and the lone electron pairs are involved in conjugation with the phenyl moieties.

In TPPA, the N1–C2 (see Scheme 1 for the definitions) bond lengths assume values of 1.410, 1.374, and 1.419 Å for the neutral, radical cation, and bi-radical species, respectively. The same bond distances in TPPAHM assume very similar values (1.410, 1.380, and 1.418 Å for neutral, radical cation, and bi-cation, respectively). For the neutral species, this distance is slightly larger than in aromatic amines and shorter than in aliphatic ones. We underline the sensible decrease of this bond distance, in going from the neutral to the radical cationic system that occurs in both molecules. In the second ionization process, the N1–C2 bond lengths assume almost the same values with that in the neutral species for both TPPA and TPPAHM systems. Other sensible variations that the ionization process induces in the geometrical parameters are found in the torsional angles. As indicated in the Table 1, the major variation concerns the $\Psi 1$ angle that in the neutral form assumes a value of 41.8° (TPPA) and 40.7° (TPPAHM) that becomes 24.7° and 26.9° for TPPA and TPPAHM radical cations, respectively. Concerning the N1–C3 bond, connecting the nitrogen atom with the peripheral phenyl moiety, our results show that during the first ionization process, it slightly increases, while decreases in the second ionization. The C4–N2 distance in TPPAHM decreases during the formation of the radical cation and continues to decrease upon the second ionization. From these data, it seems that the N1 center is more involved in the first ionization, while the N2 atom is more involved in the second ionization process. Looking at the C5–O bond, we note that both ionization processes cause a decrease in the length. The C–C distances of the phenyl rings correspond to that expected for delocalized aromatic moieties.

Comparison between the computed and crystallographic structures [11] for neutral and radical TPPA species is satisfactory for the bond distances and valence angles, while discrepancies are found for the dihedral angles (see Table 1). The same trend has been noted in a previous DFT

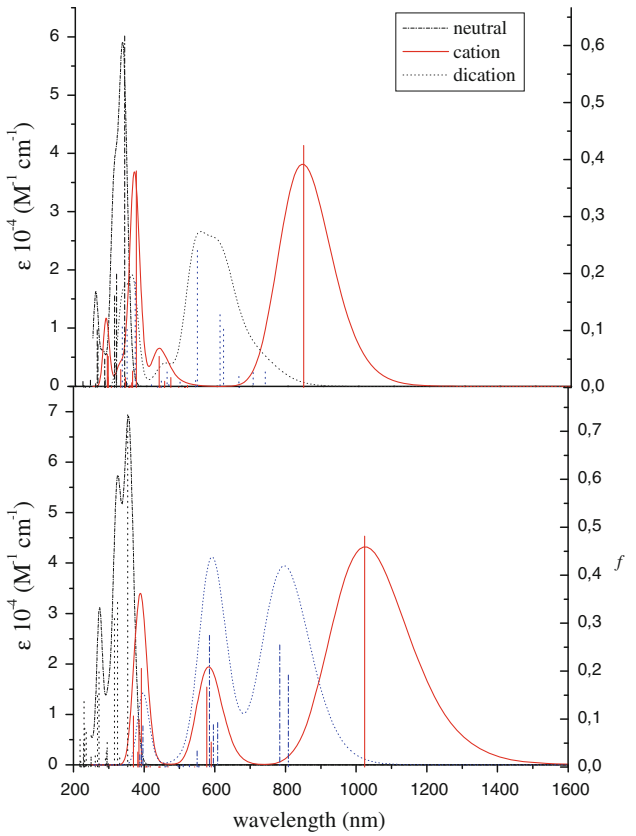

Fig. 3 TDDFT simulated spectra of TPPA (*top*) and TPPAHM (*bottom*)

study employing a different exchange–correlation functional (BPW91) [11]. If we consider that in solid state, there is a different environment (intermolecular interactions) and that around the considered dihedral angles the potential energy profile is flat, these discrepancies can be justified.

The theoretical predictions for the geometrical parameters of TPPAHM, for which experimental data are absent, follow the trends of the parent TPPA and give indications regarding the geometry of the substituted moiety as well as a useful guideline for future crystallographic measurements.

The hole transport process can be approximated as an electron transfer from a neutral molecule N to a neighboring radical cation N^+:N(a) + N(b)$^+$ → N(a)$^+$ + N(b).

As it is evident the reactants and the products in this reaction are the same, and the reaction Gibbs free energy is zero. It was pointed out [42, 43] that, neglecting the contributions arising from the polarization of the medium and from molecular vibrations, the activation energy (ΔG*) for this intermolecular charge transfer should be related with the re-organization energy (λ) through the relation $\Delta G^* = \lambda/4$. The re-organization energy is directly associated with the geometric rearrangement in going from neutral to charged systems and from charged to neutral ones. From the computations of the vertical and adiabatic ionization potentials and electron affinities (see Fig. 1), we obtain a reorganization energy values of 0.36 and 0.29 eV for TPPA and TPPAHM, respectively. These values account for a sensible geometrical relaxation process occurring in both systems as previously discussed. In a recent study [42], the λ values have been associated with the electron–hole mobility, observing that a decrease in the reorganization energy corresponds to an increase in the electron–hole mobility. On the basis of our results, we can predict a higher electron–hole mobility for the newly synthesized TPPAHM molecule compared to its TPPA counterpart.

3.2 UV–vis–NIR spectra

Spectroelectrochemical experiments have been performed in order to evaluate the optical properties of TPPA and TPPAHM electrochromic systems. The obtained spectra are shown in Fig. 2a (TPPA) and b (TPPAHM).

Without the applied electric field, the optical spectrum of TPPA is characterized by only one strong absorption peak in the B-band region. Increasing the applied voltage from 0.0 to 2.4 V, a new broad band centered around 820 nm gradually increases in intensity, and the maximum absorption peak is located at 840 nm when the applied voltage reaches its higher value (2.8 V). This band is due to an intervalence charge-transfer (IV-CT) excitation with a photoexcited electron transfer from a neutral triphenylamine center to the corresponding radical cation ones. Upon oxidation, another less intense transition appears at 402 nm. The computed TD-DFT spectrum (see Table 2) of the neutral TPPA gives also strong intensity transitions in the B-region of the spectrum (the maximum peak at 335 nm has a value of oscillator strength of 0.62). The simulated spectra show that the main peak is due to a HOMO → LUMO + 1 transition (see Table 2; Figs. 3, 4). In the simulated spectrum of the TPPA radical cation, the B-band is shifted to the lower energy value (368 nm) and the IV-CT peak is located at 842 nm with an oscillator strength value of 0.42. The analysis of the orbital transition (Fig. 4) clearly indicates its HOMO-1 → LUMO nature (96.8 %). The peak at 466 nm is assigned to a transition from an internal orbital (HOMO-9) to the LUMO one.

The newly synthesized TPPAHM molecule differs from TPPA due to the presence in *para* position of the external phenyl rings of electron-donating groups (O–CH3 and –NCOR). It was previously shown that the presence of these meta O–CH3 groups in triarylamine-like electrochromic systems prevents coupling reactions and lowers the oxidation potential [19, 44]. Thus, we will expect a pronounced NIR response in this newly synthesized

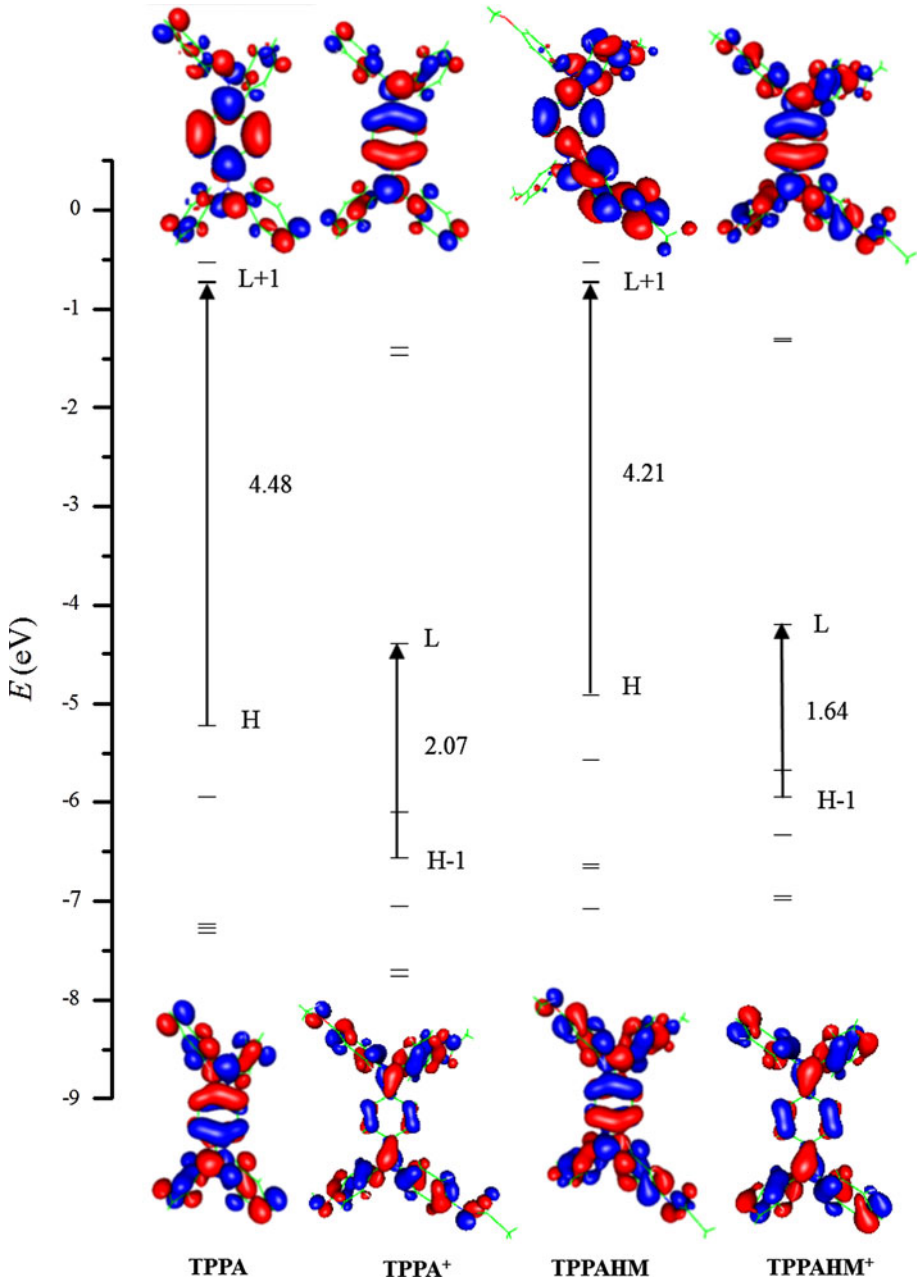

Fig. 4 Partial energetic diagram (eV) for the highest occupied and lowest virtual unoccupied molecular orbitals of molecules TPPA and TPPAHM (neutral and cationic forms). The orbital compositions are reported for the most intense transitions

system. The results of the spectrochemical experiments are reported in Fig. 2. The spectrum feature, in the neutral species, essentially shows the presence of an intense B-band at about 360 nm. The computed counterpart (see Table 2) gives almost the same spectral features with one strong peak due to the HOMO → LUMO + 1 π–π^* orbital transition at 356 nm (see Fig. 4). When the applied electric field reaches the value of 0.7 V, two new bands appear in the visible region. Upon oxidation (increasing the applied voltage up to 1.8 V), the intensity of these new absorption transitions increases, having the maximum absorption wavelength at 424 and 580 nm. The broad absorption NIR band centered at 1,040 nm was the characteristic result due to IV-CT excitation associated with the electron transfer during the oxidation of TPPAHM. The simulated TD-DFT spectra agree well with the experimental evidence as shown in Table 2 and Fig. 3. In particular, the DFT NIR peak reaches the maximum intensity (0.48) at 1,025 nm, and the transition is mainly (97.9 %) HOMO-1 → LUMO in nature (Fig. 4). The transition at 580 nm and with an oscillator strength value of 0.17 is essentially due to the HOMO-4 → LUMO transition.

Although in our experimental conditions we do not note the presence of a second oxidation process until an applied voltage of about 5 V, we have simulated the spectra for both TPPA and TPPAHM di-cations as reported in Table 2

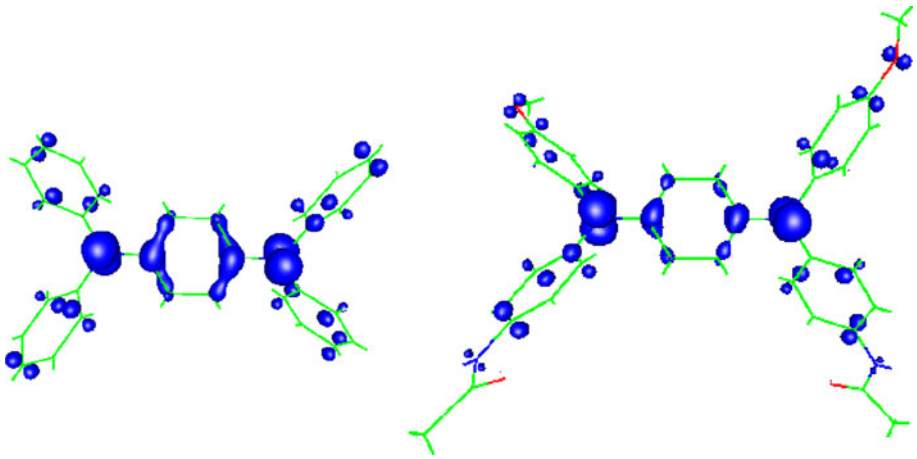

Fig. 5 Spin density contour plot for $TPPA^{+}$ (*left*) and $TPPAHM^{+}$ (*right*) (isodensity value of 0.005 a.u.)

and Fig. 3. The TPPA di-cation shows essentially a broad peak in the visible region that contains different transitions between the internal orbital and the LUMO and LUMO + 1 orbital with the maximum intensity located at 541 nm. Another less intense band is present around 280 nm. As in previous experiments, on other tetraphenylamine derivatives [10], also in our computed spectrum, the NIR band disappears when the second oxidation process occurs. Contrary to that of TPPA, the spectrum of TPPHM di-cation has a different behavior showing three different bands. The first and less intense is centered at 400 nm, the second reaches its maximum intensity (0.88) at 599 nm, and the last has oscillator strength of 0.26 at 786 nm. The last two intense bands are due to transition between orbital that lies down in energy than the frontier orbitals and LUMO and LUMO + 1 empty orbitals. Also in this case, the IV-CT NIR band is absent. We hope that these indications can be useful for the spectral identification of di-cation species in solutions of TPPA and TPPAHM molecules.

Looking at the orbital energy diagram reported in Fig. 4, in both molecules, the appearance of the NIR transition can be correlated with the lowering of the orbital energies in going from the neutral to the cation radical species.

The oxidation mechanism of triarylamine-like electrochromic systems has been the subject of many previous publications [20, 45–47]. In the major part of these works, it is supposed that the first oxidation is due to the removal of an electron from the nitrogen atom with the larger electron density, while the second one derives from the removal of a second electron from the other nitrogen atom. Recently, Wu et al. [16], in order to explain the spectrochemical behavior of a series of fluorine-based conjugated polymers containing propeller-shape di-triarylamine, have proposed an other mechanism for which the first electron must be removed by the HOMO orbital instead from the nitrogen lone pair and the second from the SOMO orbital. This proposal is based on coupling the spectrochemical data by the net charges of neutral and oxidized states calculated at the B3LYP/6-31G* level of theory. Following this strategy, we have computed, by using our computational protocol, the natural bond charges and the spin density (Fig. 5) for the neutral, cation radical, and di-cation of the TPPA and TPPAHM studied systems. From our data, it is evident that in both systems, although the N atom loss 0.11|e| (TPPA) and 0.10|e| (TPPAHM) in going from the neutral to the cation radical, these quantities are not sufficient to assert that the oxidation is mainly generated by this atom. Looking at the other net charges of the atoms surrounding the nitrogen, we note other loss of charge especially in the carbon located in the phenyl moiety that links the two nitrogen centers. Furthermore, from the orbital composition of the LUMO orbital in the neutral species (See Supplementary Informations Fig. 6), we note, in both molecules, a strong involvement of the nitrogen in the formation of the phenyl π system. Similar results are obtained from the analysis of the spin density distribution as shown in Fig. 5. On the basis of these data, we can conclude that the first oxidation involves the entire LUMO π systems and not only the nitrogen atom. Concerning the second oxidation, the analysis of Table 2, as well as that of Figs. 4 and 5, suggests that the electron must be removed from the SOMO orbital created in the first oxidation process.

4 Summary

In this study, we have employed spectroelectrochemical experiments and DFT first principles computations in order to characterize a newly synthesized triarylamine electrochromic system (TPPAHM). In addition, also the TPPA has been considered. The UV–vis–NIR spectra have been registered with and without an applied electric field at

different voltages. On the basis of our results, we can draw the following conclusions:

- Both radical cations have a delocalized IV state in which the unpaired electron is fully delocalized over the whole molecules;
- The two oxidation processes occur with the involvement of the delocalized HOMO orbital that releases an electron in the first ionization, while in the second, the electron is given by the SOMO orbital;
- The presence of electron-rich moieties on the TPPAHM shifts the NIR resonance at higher values with respect to the TPPA;
- Although the used hybrid exchange–correlation functional can give an overestimation of the charge delocalization, the agreement between the calculated and experimental UV–vis–NIR spectral behavior is very satisfactory;
- The presence of a low applied voltage is able to ionize reversibly both molecules.

Acknowledgments The University of Calabria and MIUR (PRIN 2008ALLB79) are gratefully acknowledged for financial support.

References

1. Platt JR (1961) J Chem Phys 34:862
2. Monk PMS, Mortimer RJ, Rosseinsky DR (1995) Electrochromism: fundamentals and applications. VCH Weinheim, Germany
3. Monk PMS, Mortimer RJ, Rosseinsky DR (2007) Electrochromism and electrochromic devices. Cambridge University Press, Cambridge
4. Beaujuge PM, Reynolds JR (2010) Chem Rev 110:268
5. Beaupre S, Breton AC, Dumas J, Leclerc M (2009) Chem Mater 21:1504
6. Zheng J, Qiao W, Wan X, Gao JP, Wang ZY (2008) Chem Mater 20:6163
7. Barbara PF, Meyer TJ, Ratner MA (1996) J Phys Chem 100: 13148
8. Hush NS (1961) Trans Faraday Soc 57:557
9. Robin M, Day P (1967) Adv Inorg Radiochem 10:247
10. Yen HJ, Liou GS (2009) Chem Mater 21:4062
11. Szeghalmi AV, Erdmann M, Engel V, Schmitt M, Amthor S, Kriegich V, Noll G, Stahl R, Lambert C, Leusser D, Stalke D, Zabel M, Popp J (2004) J Am Chem Soc 126:7834
12. Coropceanu V, Gruhn NE, Barlow S, Lambert C, Durivage JC, Bill TG, Noll G, Marder SR, Brédas JL (2004) J Am Chem Soc 126:2727
13. Ramos AM, Meskers SCJ, Van Hal PA, Knol J, Hummelen JC, Janssen RAJ (2003) J Phys Chem A 107:9269
14. Zhang H-G, Yu W-T, Wang L, Liu Z, Tao X-T, Jiang M-H (2005) Z Kristallogr 220:101
15. Lambert C, Noll G (1999) J Am Chem Soc 121:8434
16. Wu H-Y, Wang K-L, Liaw D-J, Lee K-R, Lai J-Y, Chen C-L (2010) J Polym Sci Part A: Polym Chem 48:3913
17. Chiu KY, Su T-H, Huang CW, Liou G-S, Cheng S-H (2005) J Electroan Chem 578:283
18. Yeh SJ, Tsai CY, Huang C-Y, Liou G-S, Cheng S-H (2003) Electrochem Commun 5:373
19. Hirao Y, Ito A, Tanaka K (2007) J Phys Chem A 111:2951
20. Selby TD, Kim K-Y, Blackstock SC (2002) Chem Mater 14:1685
21. Barlow S, Risko C, Coropceanu V, Tucker NM, Jones SC, Levi Z, Khrstalev VN, Antipin MY, Kinnibrugh TL, Timofeeva T, Marder SR (2005) Chem Commun 6:764
22. Low PJ, Paterson MAJ, Puschmann H, Goeta AE, Howard JAK, Lambert C, Cherryman JC, Tackley DR, Leeming S, Brown B (2004) Chem Eur J 10:83
23. Tsutsumi H, Nakagawa Y, Tamura K (1995) Sol Energy Mater Sol Cells 39:341
24. Leventis N, Chung Y (1998) U.S. Patent 5818636
25. Nishikitani Y, Uchida S, Asano T, Minami M, Oshima S, Ikai K, Kubo T (2008) J Phys Chem C 112:4372
26. Ahlrichs R, Bär M, Häser M, Horn H, Kölmel C (1989) Chem Phys Lett 162:165
27. Ernzerhof M, Scuseria GE (1999) J Chem Phys 110:5029
28. Adamo C, Barone V (1999) J Chem Phys 110:6158
29. Schaefer A, Horn H, Ahlrichs R (1992) J Chem Phys 97:2571
30. Eichkorn K, Weigend F, Treutler O, Ahlrichs R (1997) Theor Chem Acc 97:119
31. Bauersnschmitt R, Ahlrichs R (1996) Chem Phys Lett 256:454
32. Casida ME (1995) In: Chong DP (ed) Recent advances in density functional methods Part I. Word Scientific, Singapore
33. Quartarolo AD, Russo N, Sicilia E (2006) Chem Eur J 12:6797
34. Quartarolo AD, Sicilia E, Russo N (2009) J Chem Theory Comput 5:1849
35. Quartarolo AD, Lanzo I, Sicilia E, Russo N (2009) Phys Chem Chem Phys 11:4586
36. Lanzo I, Quartarolo AD, Russo N, Sicilia E (2009) Photochem Photobiol Sci 8:386
37. Jacquemin D, Mennucci B, Adamo C (2011) Phys Chem Chem Phys 13:16987
38. Klamt A, Jonas V (1996) J Chem Phys 105:9972
39. Klamt A (1996) J Phys Chem 100:3349
40. Renz M, Thellacker K, Lambert C, Kaupp M (2009) J Am Chem Soc 131:16292
41. Nelsen SF, Ismagilov RF, Trieber DA (1997) Science 278:846
42. Sakarnane K, Motoda M, Sugimoto M, Sakaki F (1999) J Phys Chem A 103:5551
43. Malagoli M, Brédas JL (2000) Chem Phys Lett 327:13
44. Yen H-J, Lin H-Y, Liou G-S (2011) Chem Mater 23:1874
45. Chen WH, Wang KL, Liaw DJ, Lee KR, Lai JY (2010) Macromolecules 43:2236
46. Grazulevicius JV, Strohriegl P, Pielichowski J, Pielichowski K (2003) Prog Polym Sci 28:1297
47. Ito A, Ino H, Tanaka K, Kanemoto K, Kato T (2002) Org Chem 67:491